

CrossMark  
click for updates

Cite this: DOI: 10.1039/c6cy02585d

## Hydrogenation/oxidation triggered highly efficient reversible color switching of organic molecules†

Xiao Zhou, Yi-Fan Jiang, Hong-Li Guo, Xin Wang, Ya-Nan Liu,  
M. Imran and An-Wu Xu\*

Catalytic hydrogenation and oxidative dehydrogenation reactions are fundamental and significant processes in organic transformation, and reversible color switching of organic redox dyes finds potential applications in rewritable paper, sensing devices, data recording and security feature technologies. In this study, we report an interesting result of reversible hydrogenation and oxidative dehydrogenation of a redox dye over a Pd–ZnO<sub>1-x</sub> hybrid nanocatalyst under ambient conditions. Thionine (TH<sup>+</sup>) is used as a model compound to evaluate the catalytic performance. The reversible color switching between purple thionine (TH<sup>+</sup>) and colorless leuco-thionine (LTH) depends on the reducing or oxidizing environments. Our newly developed Pd–ZnO<sub>1-x</sub> nanocatalyst exhibits high catalytic activity for the hydrogenation of TH<sup>+</sup> with a turnover frequency (TOF) as high as 397 h<sup>-1</sup> under H<sub>2</sub> (1 bar). The oxidative dehydrogenation of LTH is performed under 1 bar O<sub>2</sub> flow in the same reaction system. The Pd–ZnO<sub>1-x</sub> nanocatalyst readily adsorbs and subsequently dissociates O<sub>2</sub> to oxidize LTH to the original purple colored TH<sup>+</sup> with higher efficiency. The abundant oxygen vacancies on ZnO<sub>1-x</sub> nanorods and strong metal-support interaction (SMSI) promote the adsorption and subsequent dissociation of molecular hydrogen and oxygen leading to high catalytic activity. This novel reversible color switching of organic dyes can be performed successively for more than 10 cycles in a one pot-fashion using a Pd–ZnO<sub>1-x</sub> nanocatalyst with a small loss in performance. The highly efficient reversible color switching of TH<sup>+</sup>/LTH over the Pd–ZnO<sub>1-x</sub> nanocatalyst provides a state-of-the-art protocol to find practical applications as printing inks for rewritable paper and in sensing and security feature devices.

Received 11th December 2016,  
Accepted 18th February 2017

DOI: 10.1039/c6cy02585d

rsc.li/catalysis

## Introduction

Catalytic hydrogenation and oxidative dehydrogenation reactions have been extensively utilized in the chemical industry for the production of pharmaceuticals and fine chemicals.<sup>1–3</sup> Organic redox dyes are capable of undergoing a reversible color change under suitable conditions, which has attracted much attention for potential applications in rewritable paper, data recording, sensing devices, and security feature technologies.<sup>4–6</sup> Recently, a photoreversible color switching system that integrates the photocatalytic properties of TiO<sub>2</sub> nanocrystals into the redox-driven color change of organic dyes for the development of rewritable paper has been reported.<sup>7</sup> Thionine dye (TH<sup>+</sup>, thionine acetate), a purple re-

dox dye, can be reduced to a colorless leuco form (LTH) in a reducing environment.<sup>8</sup>

The past decade has witnessed increased interest in palladium (Pd) based catalysts due to their fascinating properties and practical applications in organic reactions.<sup>9–12</sup> Metal oxides have long been used as a support for noble metals to improve the activity of hydrogenation, dehydrogenation, redox and acid-catalyzed reactions. Among different supports, non-stoichiometric supports could endow noble metal nanoparticles new physicochemical properties due to electron communication and strong metal-support interaction (SMSI).<sup>13</sup> Moreover, defects often dominate the physical and chemical properties of semiconducting materials. Oxygen vacancies in metal oxides are particularly important because they generally serve as electron donors.<sup>14</sup> The increased carrier density resulting from oxygen vacancies improves the electrical conductivity and facilitates charge transfer between the metal oxide and the substrate at the interface. SMSI is closely linked to the catalytic properties of the metal involved, playing an important role in enhancing the catalytic activity in reactions such as hydrogenation.<sup>15,16</sup> The ability of SMSI using metal oxide supports to mediate the catalytic

Division of Nanomaterials and Chemistry, Hefei National Laboratory for Physical Sciences at Microscale Department, Department of Materials Science and Engineering, University of Science and Technology of China, Hefei 230026, P.R. China. E-mail: anwuxu@ustc.edu.cn

† Electronic supplementary information (ESI) available: Additional TEM, EPR spectra, and UV-vis spectra. See DOI: 10.1039/c6cy02585d

behavior of supported metal nanoparticles is of great importance in the catalytic field with both scientific and commercial significance.<sup>17</sup> Hydrogenation of organic dyes is often used for the evaluation of catalytic activity, because of their obvious color change and convenient measurements by UV-vis spectroscopy.<sup>18,19</sup> Metal oxide supported Pd nanoparticles have shown excellent catalytic performance for hydrogenation. This type of hybrid nanocatalyst is also employed for the activation of molecular oxygen (O<sub>2</sub>) in various oxidation reactions, including oxidative dehydrogenation reactions,<sup>20</sup> CO oxidation,<sup>21</sup> glucose oxidation,<sup>22</sup> and oxidative coupling.<sup>23</sup> Some model studies have shown that the adsorption and dissociation of H<sub>2</sub> and O<sub>2</sub> on the surfaces of metal oxide supported Pd nanoparticles have much influence on the catalytic activities.<sup>24–26</sup>

Herein, we synthesize oxygen deficient ZnO<sub>1-x</sub> nanorods as a support for loading noble metal nanoparticles to evaluate the catalytic performance using redox thionine dye as a probe. The activated hydrogen over Pd-ZnO<sub>1-x</sub> hybrid nanostructures can rapidly bleach the original purple color of TH<sup>+</sup> by the hydrogenation process. Notably, the formed colorless leuco-thionine (LTH) can be quickly switched back to purple colored TH<sup>+</sup> through the oxidative dehydrogenation process with activated oxygen over the Pd-ZnO<sub>1-x</sub> nanocatalyst. This strategically tailored catalyst not only shows high catalytic reduction of thionine to leuco-thionine but also exhibits efficient activation of molecular oxygen for oxidative dehydrogenation in a one-pot reaction system. The Pd-ZnO<sub>1-x</sub> hybrid nanocatalyst proves to be a promising candidate for highly efficient, multifunctional hydrogenation/oxidative dehydrogenation reactions, which may find applications in data recording, data security, rewritable paper and organic transformations.

## Experimental section

### Materials

Na<sub>2</sub>PdCl<sub>4</sub> was purchased from Alfa Aesar. Thionine acetate and hydroxyethyl cellulose (HEC) were purchased from Sigma-Aldrich. Zinc chloride (ZnCl<sub>2</sub>), tin tetrachloride (SnCl<sub>4</sub>), ammonium chloride (NH<sub>4</sub>Cl), zinc powder, tin powder and potassium hydroxide (KOH) were obtained from Sinopharm Chemical Reagent Co., Ltd. All chemicals were used as received without further purification. Double distilled water was used in all experiments.

### Synthesis of the ZnO<sub>1-x</sub> nanorods and the Pd-ZnO<sub>1-x</sub> nanocatalyst

In a typical synthesis, 1 mmol of ZnCl<sub>2</sub> and 0.5 mmol of SnCl<sub>4</sub> were dissolved in distilled water (15 mL) with vigorous stirring for 15 min; then, the metallic zinc powder (1 mmol) and tin powder (0.5 mmol) were added into the aqueous solution. After stirring for another 15 min, 2 mmol of NH<sub>4</sub>Cl and 0.05 mol of KOH were added, and then the mixture was stirred for 0.5 h to obtain a homogeneous suspension. The mixed solution was transferred into a 25 mL Teflon-lined

stainless steel autoclave. The autoclave was sealed and heated at 180 °C for 15 h in an oven. After air-cooling to room temperature, the gray-colored ZnO<sub>1-x</sub> was collected by centrifugation and washed with distilled water and ethanol three times. The obtained product was dried at 60 °C in a vacuum oven. The Pd-ZnO<sub>1-x</sub> nanocatalyst was obtained by mixing 10 mL of 1.0 mg mL<sup>-1</sup> ZnO<sub>1-x</sub> NR aqueous suspension with 0.1 mL of 10 mM Na<sub>2</sub>PdCl<sub>4</sub> in a quartz tube. The nominal weight content of Pd in the composite is 1.0 wt%. The above solution was sonicated for 3 min and then irradiated for 60 min with a 260 W mercury lamp (SHG-200, Mejiro Precision Inc., Japan). A color change from grey to dark grey was observed, indicating the formation of Pd-ZnO<sub>1-x</sub> hybrid nanostructures. Finally, the product was collected by centrifugation, washed three times with distilled water, and dried at 60 °C in a vacuum oven for further experiments.

### Characterization

The X-ray powder diffraction (XRD) patterns of the samples were collected using a Rigaku/Max-3A X-ray diffractometer with Cu K $\alpha$  radiation ( $\lambda = 1.54178 \text{ \AA}$ ); the operation voltage and current were maintained at 40 kV and 200 mA, respectively. The morphologies of nanocrystals were examined by transmission electron microscopy (TEM), using a JEOL JEM12010 high resolution transmission electron microscope operated at 200 kV. High resolution TEM (HRTEM) images were obtained using a JEOL JEM12100F field emission high resolution transmission electron microscope operated at 200 kV. X-ray photoelectron spectroscopy (XPS) was performed using a Perkin-Elmer RBD upgraded PHI-5000C ESCA system. The actual content of Pd was measured using a Thermo Scientific Plasma Quad 3 inductively-coupled plasma mass spectrometer (ICP-MS) after dissolving the sample with a mixture of HCl and HNO<sub>3</sub> (3 : 1, volume ratio). The electron paramagnetic resonance (EPR) spectra were recorded on a JEOL JES-FA200 EPR spectrometer (140 K, 9064 MHz, 0.998 mW, X-band).

### Reversible hydrogenation/oxidative dehydrogenation over the Pd-ZnO<sub>1-x</sub> nanocatalyst

Typically, 0.25 mg of 1 wt% Pd-ZnO<sub>1-x</sub> hybrid catalyst and 0.1 g of HEC were dispersed in 9.3 mL of distilled water in a 25 mL quartz cell with vigorous stirring for 5 min; then 0.7 mL of TH<sup>+</sup> (1 mM) was added. To remove the oxygen from the system, the quartz cell was sealed with a rubber cap and then continually purged with nitrogen for at least 30 min before reaction, and an adsorption/desorption equilibrium between the catalyst and TH<sup>+</sup> could be guaranteed. The system was sequentially bubbled with hydrogen and then oxygen at a flow rate of 10 mL min<sup>-1</sup> measured using a mass flow controller (D07-19B, Sevenstar Electronics Co., Ltd., Beijing). The concentration of TH<sup>+</sup> at different time intervals was monitored by the absorption peak at  $\lambda = 600 \text{ nm}$  using a U-3900/3900H UV-vis spectrophotometer (Hitachi).

## Reversible color switching of the spotted pattern

A  $\text{TH}^+$ /HEC/Pd-ZnO<sub>1-x</sub> mixed solution was prepared using the same procedure as described above. 30  $\mu\text{L}$  of  $\text{TH}^+$ /HEC/Pd-ZnO<sub>1-x</sub> solution was dropped onto a hydrophobic Teflon plate/film to obtain a spotted pattern. Then, the spotted pattern was transferred to a container charged with 1 bar  $\text{H}_2/\text{O}_2$  for reversible color switching.

## Results and discussion

Oxygen vacancy abundant ZnO<sub>1-x</sub> nanorods (NRs) were first prepared by hydrothermal treatment; then, Pd-ZnO<sub>1-x</sub> hybrid nanostructures were synthesized by a photo-reduction deposition method, in which photo-induced electrons from ZnO<sub>1-x</sub> were employed to reduce  $\text{PdCl}_4^{2-}$  ( $\text{Pd}^{2+}$ ) on the ZnO<sub>1-x</sub> surface (see the ESI<sup>†</sup>). The surface of Pd nanoparticles (NPs) is clean since no additional surfactants were added. The crystal structure of the as-prepared oxygen vacancy-rich ZnO<sub>1-x</sub> support and Pd-ZnO<sub>1-x</sub> nanocatalyst was investigated using the X-ray diffraction (XRD) pattern. As shown in Fig. 1, the diffraction peaks from the oxygen deficient ZnO<sub>1-x</sub> sample can be readily indexed to the hexagonal wurtzite structure of zinc oxide crystals (JCPDS no. 36-1451). After the deposition of Pd NPs, the diffraction peaks for Pd were not observed likely due to the ultralow Pd (nominal content: 1 wt%) loading.

Fig. 2a and b display the transmission electron microscopy (TEM) images of the bare ZnO<sub>1-x</sub> NRs and Pd-ZnO<sub>1-x</sub> sample. The high resolution TEM (HRTEM) images further reveal the formation of the Pd-ZnO<sub>1-x</sub> hybrid nanocatalyst (Fig. 2c and d). Ultrasmall, uniform and highly dispersed Pd NPs (<4.5 nm) are clearly observed on the surface of ZnO<sub>1-x</sub> NRs (the inset in Fig. 2c shows the size distribution of Pd particles). The as-synthesized ZnO<sub>1-x</sub> sample displays a rod-like shape with an average diameter of 125 nm (Fig. 2a and S1<sup>†</sup>). The HRTEM image clearly shows that Pd NPs and ZnO<sub>1-x</sub> NRs have a single crystalline structure (Fig. 2d). The

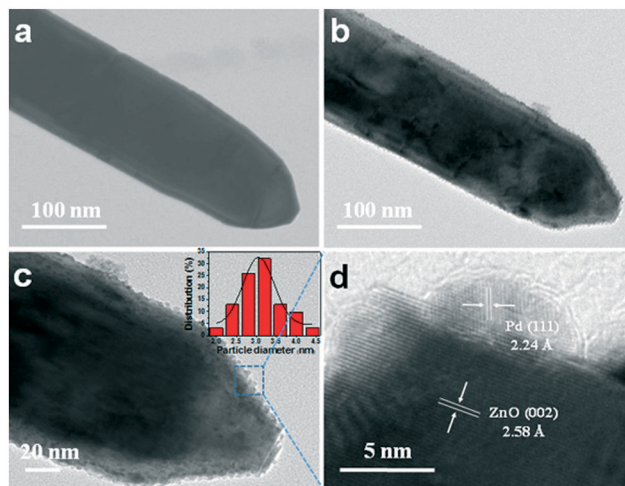


Fig. 2 TEM images of a ZnO<sub>1-x</sub> NR (a) and a Pd-ZnO<sub>1-x</sub> hybrid catalyst (b and c). HRTEM image of the Pd-ZnO<sub>1-x</sub> nanocatalyst (d). The inset in (c) shows a size distribution of the Pd nanoparticles supported on ZnO<sub>1-x</sub> NRs.

clear lattice spacing of 0.224 nm corresponds to the planar distance of the Pd {111} plane. The lattice fringe spacing of 0.258 nm is assigned to the hexagonal ZnO<sub>1-x</sub> {002} plane.

X-ray photoelectron spectroscopy (XPS) analysis was performed to reveal the chemical states and composition of the Pd-ZnO<sub>1-x</sub> catalyst. The results from the XPS analysis confirm the presence of zinc, palladium and oxygen (Fig. 3a). Fig. 3b shows the high resolution XPS spectra of Pd 3d; the peaks at 335.6 and 340.9 eV are attributed to the 3d<sub>5/2</sub> and 3d<sub>3/2</sub> binding energies of the zero-valent state of metallic Pd, respectively. The corresponding binding energy of Pd 3d has a positive shift by about 0.7 eV compared to the standard peak position,<sup>27</sup> indicating the SMSI between the Pd NPs and the ZnO<sub>1-x</sub> NRs.<sup>28</sup> The peaks that appeared at 337.2 and 342.5 eV correspond to the 3d<sub>5/2</sub>

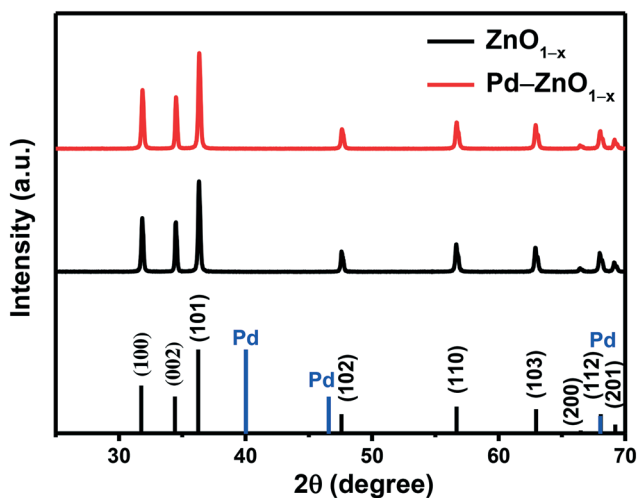


Fig. 1 XRD patterns of the as-prepared ZnO<sub>1-x</sub> NRs and Pd-ZnO<sub>1-x</sub> nanocatalyst. The PDF standard card for the hexagonal zinc oxide crystal and cubic Pd is shown at the bottom.

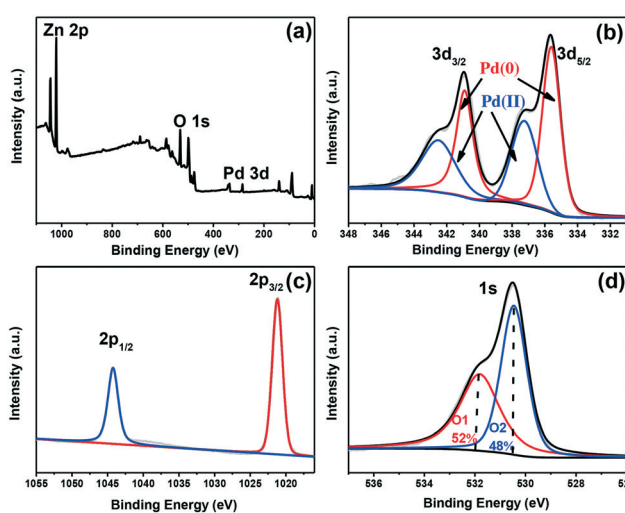


Fig. 3 XPS spectra of the Pd-ZnO<sub>1-x</sub> nanocatalyst: (a) the survey spectrum, (b) Pd 3d spectra, (c) Zn 2p spectrum and (d) O1s spectrum.

and  $3d_{3/2}$  levels of  $\text{Pd}^{2+}$ , respectively.<sup>29</sup> The atomic ratio of  $\text{Pd}(0)$  to  $\text{Pd}(II)$  is estimated to be about 1:0.7. The peaks at 1021.9 and 1044.2 eV are assigned to  $\text{Zn } 2p_{3/2}$  and  $\text{Zn } 2p_{1/2}$  (Fig. 3c), respectively.<sup>30</sup> The O 1s electron binding energy peak, as shown in Fig. 3d, can be fitted well by two Gaussian components having centres at 530.4 and 531.8 eV.<sup>31</sup> The low binding energy component accounting for about 48% of the O 1s spectrum is ascribed to the  $\text{O}^{2-}$  ions in the wurtzite structure with hexagonal  $\text{Zn}^{2+}$  ions arranged periodically. The component at the high binding energy region, accounting for the remaining 52%, is related to the O 1s in the zinc hydroxide species and adsorbed or chemisorbed oxygen species due to surface hydroxyl groups.<sup>32</sup> The atomic O content (44.7%) calculated from the XPS data is less than the Zn content (55.3%) in the  $\text{ZnO}_{1-x}$  ( $x = 0.19$ ,  $x$  stands for the concentration of oxygen vacancies) sample, which demonstrates the existence of abundant oxygen vacancies in  $\text{ZnO}_{1-x}$  NRs. This is in good agreement with the electron paramagnetic resonance (EPR) measurements (Fig. S2<sup>†</sup>). The  $\text{ZnO}_{1-x}$  sample gives rise to a very strong EPR signal at  $g = 2.001$ , which was previously identified as electrons trapped on surface oxygen vacancies.<sup>33,34</sup> These free electrons provided by the oxygen vacancies in the support can transfer to Pd, promoting its catalytic performance. The actual Pd content in the  $\text{Pd-ZnO}_{1-x}$  sample was determined to be 0.9 wt% by inductively-coupled plasma mass spectrometry (ICP-MS), which is close to the nominal content (1 wt%) in the experiment.

Pd-based nanomaterials have been extensively used for hydrogenation reactions because of their higher catalytic activities, but their high-cost and limited availability forces us to find an alternative option by using promoter-supported ultralow Pd loadings. The use of a non-stoichiometric support for noble metal particles could provide new physico-chemical properties by SMSI (as confirmed by the XPS spectra) to improve the catalytic activities. We synthesized oxygen-vacancy-rich  $\text{ZnO}_{1-x}$  NRs as a support and a promoter for Pd NPs, because it is reported that the zinc oxide itself can function in the dissociation of molecular hydrogen producing hydrogen species capable of participating in hydrogenation reactions.<sup>35</sup> The hydrogenation of thionine ( $\text{TH}^+$ ) was performed over the  $\text{Pd-ZnO}_{1-x}$  hybrid catalyst under an initial hydrogen pressure of 1 bar and at room temperature. The purple colored  $\text{TH}^+$  has an absorption maximum at 600 nm (Fig. 4a). Upon hydrogenation, the color of the aqueous  $\text{TH}^+$  solution rapidly changed from purple to colorless with increasing reaction time, which corresponds to the reduction of  $\text{TH}^+$  to leuco-thionine (LTH), and completely disappeared after 5 min (Fig. 4a). The hydrogenation activity of the  $\text{Pd-ZnO}_{1-x}$  hybrid nanocatalyst was evaluated by the calculation of turnover frequency (TOF, defined as moles of  $\text{TH}^+$  molecules per mole of the Pd catalyst per hour), resulting in a TOF value of  $397 \text{ h}^{-1}$ . This high TOF value strongly suggests the enhanced catalytic activity of  $\text{Pd-ZnO}_{1-x}$  for the hydrogenation of thionine. The catalytic hydrogenation over  $\text{Pd-ZnO}$  (commercial ZnO without oxygen vacancies) was also performed for comparison, and the results are shown in Fig.

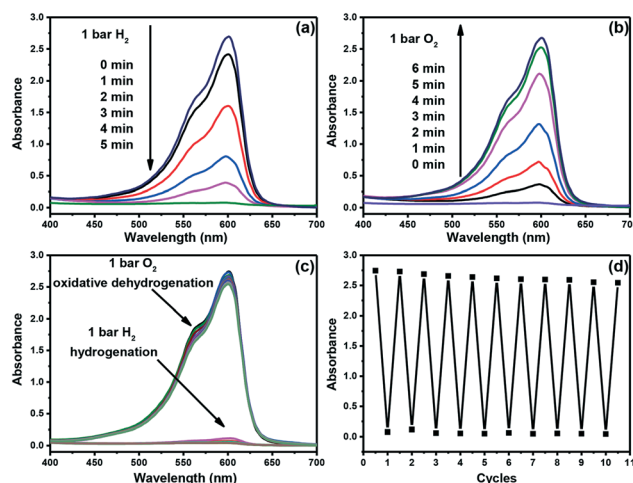


Fig. 4 Reversible hydrogenation/oxidative dehydrogenation of the redox thionine dye over the  $\text{Pd-ZnO}_{1-x}$  catalyst exposed to a hydrogen atmosphere and an oxygen atmosphere at room temperature. (a) UV-vis spectra showing the hydrogenation process under 1 bar  $\text{H}_2$ . (b) UV-vis spectra showing the oxidative dehydrogenation process under 1 bar  $\text{O}_2$ . (c) UV-vis spectra of the reaction solution after each  $\text{H}_2$  and  $\text{O}_2$  exposure for 10 continuous cycles. (d) The absorption intensity at 600 nm recorded after each  $\text{H}_2$  and  $\text{O}_2$  exposure for 10 continuous cycles.

S3.<sup>†</sup>  $\text{Pd-ZnO}_{1-x}$  with oxygen vacancies exhibits a 4 times higher activity as compared to  $\text{Pd-ZnO}$  without oxygen vacancies; this further confirms that  $\text{ZnO}_{1-x}$  with abundant oxygen vacancies plays a promoter role in the enhancement of  $\text{TH}^+$  hydrogenation. Previous report showed that the hydrogenation rate is linearly dependent on the concentration of oxygen vacancies, as the oxygen deficient surface activates molecular  $\text{H}_2$  easily from kinetic and thermodynamic aspects.<sup>36</sup> The presence of oxygen vacancies leads to an increased adsorption energy of molecular hydrogen and lowers the energy barrier associated with the cleavage of the H-H bond.<sup>37</sup> Minute amounts of Pd NPs loaded on the surface of the oxygen deficient  $\text{ZnO}_{1-x}$  promoter significantly enhance the catalytic activity due to the strong metal support interaction and synergistic effect.

Following the boosted catalytic activity of the  $\text{Pd-ZnO}_{1-x}$  catalyst for the hydrogenation of thionine, we assessed its performance for oxidative dehydrogenation of leuco-thionine (LTH) in a one-pot reaction. Pd-based nanomaterials have been widely used in oxidation reactions,<sup>38</sup> as the adsorption and dissociation of  $\text{O}_2$  on the surfaces of Pd are well known to function in a range of selective oxidative cleavages.<sup>39</sup> LTH was oxidized back to thionine ( $\text{TH}^+$ ) over the  $\text{Pd-ZnO}_{1-x}$  nanocatalyst in the presence of hydroxyethyl cellulose (HEC). HEC added in the solution can significantly slow down the oxidation process of LTH through hydrogen bonding between the  $-\text{NH}_2$  groups on LTH and the  $-\text{OH}$  groups on HEC molecules (Fig. S4 and S5<sup>†</sup>).<sup>7</sup> After hydrogenation was terminated, the system was then exposed to 1 bar oxygen. The absorption spectra of the colorless aqueous LTH/HEC/ $\text{Pd-ZnO}_{1-x}$  system have completely recovered after 6 min under an initial oxygen pressure of 1 bar at room temperature (Fig. 4b). The colorless

leuco-thionine was quickly switched back to the purple colored thionine by the activated  $O_2$  over Pd-ZnO<sub>1-x</sub>, inducing back electron transfer from LTH to oxygen. Meanwhile, the Pd-ZnO (commercial ZnO without oxygen vacancies) catalyst exhibits a lower oxidation activity of LTH, and the original purple color cannot be completely recovered even after 60 min (Fig. S6†). The efficient oxidative dehydrogenation activity of the Pd-ZnO<sub>1-x</sub> nanocatalyst can be attributed to the defect promoting effect, as the oxygen vacancies in Pd-ZnO<sub>1-x</sub> enhance the oxygen activation, which further facilitates the activation of a N-H bond of LTH; this is a key step in the Mars-van Krevelen mechanism and increases the rate of LTH interaction with the lattice oxygen.<sup>40</sup>

To evaluate the stability of the Pd-ZnO<sub>1-x</sub> nanocatalyst for potential applications, the hydrogenation/oxidative dehydrogenation processes were repeated by sequentially exposing the system to a hydrogen atmosphere and an oxygen atmosphere. As shown in Fig. 4c, the recorded spectra nearly overlap, indicating the complete reversible conversion between LTH and TH<sup>+</sup>. Fig. 4d plots the intensity of absorption maximum (600 nm) against cycles of exposure to hydrogen and oxygen, showing an almost complete reversibility of hydrogenation and oxidative dehydrogenation processes. The Pd-ZnO<sub>1-x</sub> hybrid catalyst was able to be recycled at least ten times with a small loss in performance, which is considered as a prerequisite for practical applications. Based on these results, it is noted that the reversible color switching property could be used to develop rewritable paper and sensing and security feature devices. To realize this possibility, a spotted pattern was obtained by drop-casting aqueous dispersion of TH<sup>+</sup>/HEC/Pd-ZnO<sub>1-x</sub> on Teflon substrates. Thionine (TH<sup>+</sup>) exhibits a bright purple color under an oxidizing environment; the photograph of micro-droplet arrays of 'USTC' is vividly displayed for writing information. Upon changing to a reducing environment (1 bar H<sub>2</sub>), purple TH<sup>+</sup> was reduced into colorless LTH; the pattern completely disappeared for erasing information (see Video S1 in the ESI†). When the system was switched to an oxidative environment (1 bar O<sub>2</sub>), the pattern that vanished appeared quickly (see Video S2 in the ESI†). This redox-responsive actuation color switching is readily visualized for many times, as clearly shown in Fig. 5. The droplet size of the TH<sup>+</sup>/HEC/Pd-ZnO<sub>1-x</sub> mixture solution affects the color switching process; a bigger size drop takes a longer time for both color fading and color recovery processes. In addition, the concentration of Pd-ZnO<sub>1-x</sub> has a minor influence on the switching behavior (see Tables S1 and S2 in the ESI†).

In the hydrogenation process, when hydrogen was introduced into the reaction system, molecular hydrogen is thought to initially bind to the atoms of Pd nanoparticles supported on ZnO<sub>1-x</sub> nanorods *via* its H-H  $\sigma$ -bond and then dissociates,<sup>41</sup> as depicted in Fig. 6. The abundant oxygen vacancies on ZnO<sub>1-x</sub> provide additional free electrons that can be transferred to Pd, further promoting the cleavage of the H-H bond.<sup>36,39</sup> Oxygen vacancies carry unpaired electrons that could serve as effective electron donors, as confirmed by

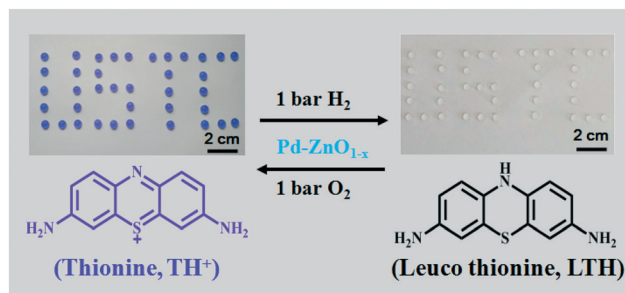


Fig. 5 Schematic illustration of the reversible hydrogenation/oxidative dehydrogenation process of TH<sup>+</sup>/LTH over a highly active Pd-ZnO<sub>1-x</sub> hybrid catalyst under ambient conditions. The insets show the photographs of micro-droplet arrays of 'USTC' in response to hydrogen and oxygen for erasing and writing information.

EPR (Fig. S2†). The transfer of free electrons from ZnO<sub>1-x</sub> to Pd enriches the electron density of metallic Pd and accelerates the hydrogenation reaction.<sup>42</sup> Hydrogen would undergo homolytic dissociation on the palladium surface into H atoms with a partially negative charge (H<sup>δ-</sup>,  $\delta$  represents the electric charge amount).<sup>43</sup> The electron donation from oxygen vacancies of ZnO<sub>1-x</sub> leads to an electron-rich Pd surface. Tuning the electronic structure of nanocatalysts is an effective strategy to optimize their catalytic activities.<sup>44,45</sup> Such an electronic effect also makes the catalytic surface favour the desorption of negatively charged H atoms (H<sup>δ-</sup>) from electron-rich Pd NPs, resulting in rapid hydrogenation of purple colored TH<sup>+</sup> to colorless LTH. For oxidative dehydrogenation reaction, oxygen activation and dissociation on the Pd-ZnO<sub>1-x</sub> nanocatalyst occur when oxygen flows into the reaction system. Oxygen can be easily dissociated on the Pd surface as the dissociation energy barrier is very small.<sup>26</sup> In the first step of oxidative dehydrogenation, O<sub>2</sub> adsorbs on the catalyst surface with a high probability in a weakly bound state and a Pd-O bond forms. Then, the hydrogen atom of the N-H bond in LTH combines with one negatively charged oxygen atom, and finally, thionine (TH<sup>+</sup>) is reproduced. The

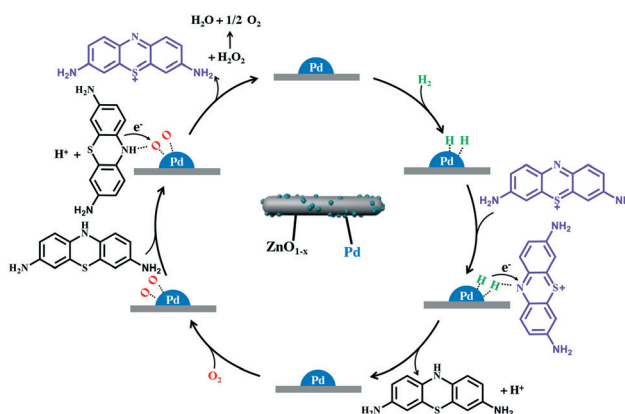


Fig. 6 Proposed reaction mechanism of one-pot reversible thionine hydrogenation and leuco-thionine oxidative dehydrogenation over a Pd-ZnO<sub>1-x</sub> nanocatalyst.

reaction of LTH with the activated oxygen regenerates Pd(0) species, along with the formation of H<sub>2</sub>O. Taken together, the strong metal support interaction between Pd and ZnO<sub>1-x</sub> with abundant oxygen vacancies plays an important role in highly efficient reversible hydrogenation/oxidative dehydrogenation of redox thionine molecules.

## Conclusions

In this work, we have developed a novel Pd-ZnO<sub>1-x</sub> hybrid nanocatalyst which exhibits high catalytic activity for both hydrogenation and oxidative dehydrogenation reactions performed successively in a one pot-fashion. Thionine dye is used as a probe to evaluate the catalytic performance of Pd-ZnO<sub>1-x</sub> by sequential exposure of the reaction solution to oxidizing and reducing environments. The enhanced activities are attributed to abundant oxygen vacancies in ZnO<sub>1-x</sub> and the strong metal-support interaction in Pd-ZnO<sub>1-x</sub>, which not only provide free electrons to Pd nanoparticles but also lower the energy barrier for the adsorption and subsequent dissociation of H<sub>2</sub> and O<sub>2</sub>. The catalytic performance of Pd-ZnO without oxygen vacancies is much lower as compared to that of the Pd-ZnO<sub>1-x</sub> nanocatalyst, which further confirms the role played by oxygen vacancies in the promotion of activities. The highly efficient activities of the hydrogenation and oxidative dehydrogenation reactions over the Pd-ZnO<sub>1-x</sub> hybrid nanocatalyst may find practical applications for synthesizing pharmaceuticals and fine chemicals in industry. In addition, we anticipate that this thionine/HEC/Pd-ZnO<sub>1-x</sub> reversible color switching system could be used as printing inks for rewritable paper, sensing devices, data recording and security feature technology. However, because of the poor the solubility and diffusion of H<sub>2</sub> and O<sub>2</sub>, there are still some difficulties to overcome in constructing an actual device from the solution. Our future work will focus on the practical application.

## Acknowledgements

The special funding support from the National Natural Science Foundation of China (51572253 and 21271165), the Scientific Research Grant of Hefei Science Center of CAS (2015SRG-HSC048), and the cooperation between the NSFC and the Netherlands Organization for Scientific Research (51561135011) is acknowledged.

## References

- R. Yamaguchi, C. Ikeda, Y. Takahashi and K. I. Fujita, *J. Am. Chem. Soc.*, 2009, **131**, 8410–8412.
- D. H. Ge, L. Hu, J. Q. Wang, X. M. Li, F. Q. Qi, J. M. Lu, X. Q. Cao and H. W. Gu, *ChemCatChem*, 2013, **5**, 2183–2186.
- (a) F. Buonomo, D. Sanfilippo, F. Trifiro, G. Ertl, H. Knözinger and J. Weitkamp, *Handbook of Heterogeneous Catalysis*, 1997, vol. 5, p. 2140; (b) K. Kochloefl, G. Ertl, H. Knözinger and J. Weitkamp, *Handbook of Heterogeneous Catalysis*, 1997, vol. 5, p. 2151.
- R. A. Evans, T. L. Hanley, M. A. Skidmore, T. P. Davis, G. K. Such, L. H. Yee, G. E. Ball and D. A. Lewis, *Nat. Mater.*, 2005, **4**, 249–253.
- S. Kobatake, S. Takami, H. Muto, T. Ishikawa and M. Irie, *Nature*, 2007, **446**, 778–781.
- X. S. Hou, C. F. Ke, C. J. Bruns, P. R. McGonigal, R. B. Pettman and J. F. Stoddart, *Nat. Commun.*, 2015, **6**, 6884–6892.
- W. S. Wang, N. Xie, L. He and Y. D. Yin, *Nat. Commun.*, 2014, **5**, 5459–5465.
- E. Rabinowitch, *J. Chem. Phys.*, 1940, **8**, 551–559.
- C. L. Li, T. Sato and Y. Yamauchi, *Angew. Chem., Int. Ed.*, 2013, **52**, 8050–8053.
- R. Su, R. Tiruvalam, A. J. Logsdail, Q. He, C. A. Downing, M. T. Jensen, N. Dimitratos, L. Kesavan, P. P. Wells, R. Bechstein, H. H. Jensen, S. Wendt, C. R. A. Catlow, C. J. Kiely, G. J. Hutchings and F. Besenbacher, *ACS Nano*, 2014, **8**, 3490–3497.
- J. K. Edwards, J. Pritchard, P. J. Miedziak, M. Piccinini, A. F. Carley, Q. He, C. J. Kiely and G. J. Hutchings, *Catal. Sci. Technol.*, 2014, **4**, 3244–3250.
- F. Klotter and A. Studer, *Angew. Chem., Int. Ed.*, 2014, **53**, 2473–2476.
- (a) C. M. Fan, L. F. Zhang, S. S. Wang, D. H. Wang, L. Q. Lu and A. W. Xu, *Nanoscale*, 2012, **4**, 6835–6840; (b) S. J. Tauster, *Acc. Chem. Res.*, 1987, **20**, 389–394.
- W. S. Wang, Y. F. Ye, J. Feng, M. F. Chi, J. H. Guo and Y. D. Yin, *Angew. Chem.*, 2015, **127**, 1337–1342.
- M. A. Vannice and B. Sen, *J. Catal.*, 1989, **115**, 65–78.
- J. Kijeński, P. Winiarek, T. Paryczak, A. Lewicki and A. Mikołajska, *Appl. Catal., A*, 2002, **233**, 171–182.
- (a) J. Graciani, K. Mudiyansele, F. Xu, A. E. Baber, J. Evans, S. D. Senanayake, D. J. Stacchiola, P. Liu, J. Hrbek, J. F. Sanz and J. A. Rodriguez, *Science*, 2014, **345**, 546–550; (b) S. Kuld, M. Thorhauge, H. Falsig, C. F. Elkjær, S. Helveg, I. Chorkendorff and J. Sehested, *Science*, 2016, **352**, 969–974; (c) M. B. Fichtl, J. Schumann, I. Kasatkin, N. Jacobsen, M. Behrens, R. Schlögl, M. Muhler and O. Hinrichsen, *Angew. Chem., Int. Ed.*, 2014, **53**, 7043–7047.
- S. L. Yang, C. Y. Cao, Y. B. Sun, P. P. Huang, F. F. Wei and W. G. Song, *Angew. Chem., Int. Ed.*, 2015, **54**, 2661–2664.
- K. Y. Cho, Y. S. Yeom, H. Y. Seo, P. Kumar, A. S. Lee, K. Y. Baek and H. G. Yoon, *J. Mater. Chem. A*, 2015, **3**, 20471–20476.
- L. Kesavan, R. Tiruvalam, M. H. Ab Rahim, M. I. bin Saiman, D. I. Enache, R. L. Jenkins, N. Dimitratos, J. A. Lopez-Sanchez, S. H. Taylor, D. W. Knight, C. J. Kiely and G. J. Hutchings, *Science*, 2011, **331**, 195–199.
- X. W. Xie, Y. Li, Z. Q. Liu, M. Haruta and W. J. Shen, *Nature*, 2009, **458**, 746–749.
- T. Ishida, N. Kinoshita, H. Okatsu, T. Akita, T. Takei and M. Haruta, *Angew. Chem.*, 2008, **120**, 9405–9408.
- J. Wahlen, D. E. De Vos, P. A. Jacobs and P. L. Alsters, *Adv. Synth. Catal.*, 2004, **346**, 152–164.
- M. Cargnello, J. J. Delgado Jaén, J. C. Hernández Garrido, K. Bakhmutsky, T. Montini, J. J. Calvino Gámez, R. J. Gorte and P. Fornasiero, *Science*, 2012, **337**, 713–717.

- 25 S. Mukherjee, L. N. Zhou, A. M. Goodman, N. Large, C. Ayala-Orozco, Y. Zhang, P. Nordlander and N. J. Halas, *J. Am. Chem. Soc.*, 2014, **136**, 64–67.
- 26 F. F. Wang, Z. S. Lu, L. Yang, Y. X. Zhang, Q. H. Tang, Y. M. Guo, X. M. Ma and Z. X. Yang, *Chem. Commun.*, 2013, **49**, 6626–6628.
- 27 C. D. Wagner, W. M. Riggs, L. E. Davis, J. F. Moulder and G. E. Muilenberg, *Handbook of X-ray Photoelectron Spectroscopy*, 1979, vol. 55, pp. 110–111.
- 28 A. Y. Klyushin, M. T. Greiner, X. Huang, T. Lunkenbein, X. Li, O. Timpe, M. Friedrich, M. Hävecker, A. Knop-Gericke and R. Schlögl, *ACS Catal.*, 2016, **6**, 3372–3380.
- 29 D. L. Wang, S. F. Lu, P. J. Kulesza, C. M. Li, R. D. Marco and S. P. Jiang, *Phys. Chem. Chem. Phys.*, 2011, **13**, 4400–4410.
- 30 D. R. Kumar, D. Manoj and J. Santhanalakshmi, *RSC Adv.*, 2014, **4**, 8943–8952.
- 31 T. Rakshit, S. P. Mondal, I. Manna and S. K. Ray, *ACS Appl. Mater. Interfaces*, 2012, **4**, 6085–6095.
- 32 S. Sepulveda-Guzman, B. Reerajayan, E. D. L. Rosa, A. Torres-Castro, V. Gonzalez-Gonzalez and M. Jose-Yacaman, *Mater. Chem. Phys.*, 2009, **115**, 172–178.
- 33 I. Nakamura, N. Negishi, S. Kutsuna, T. Ihara, S. Sugihara and K. Takeuchi, *J. Mol. Catal. A: Chem.*, 2000, **161**, 205–212.
- 34 H. L. Guo, Q. Zhu, X. L. Wu, Y. F. Jiang, X. Xie and A. W. Xu, *Nanoscale*, 2015, **7**, 7216–7223.
- 35 (a) K. Cheng, B. Gu, X. L. Liu, J. C. Kang, Q. G. Zhang and Y. Wang, *Angew. Chem., Int. Ed.*, 2016, **55**, 4725–4728; (b) R. J. Kokes, A. L. Dent, C. C. Chang and L. T. Dixon, *J. Am. Chem. Soc.*, 1972, **94**, 4429–4436.
- 36 J. J. Song, Z. F. Huang, L. Pan, J. J. Zou, X. W. Zhang and L. Wang, *ACS Catal.*, 2015, **5**, 6594–6599.
- 37 V. V. Kaichev, D. Teschner, A. A. Saraev, S. S. Kosolobov, A. Y. Gladky, I. P. Prosvirin, N. A. Rudina, A. B. Ayupov, R. Blume, M. Hävecker, A. Knop-Gericke, R. Schlögl, A. V. Latyshev and V. I. Bukhtiyarov, *J. Catal.*, 2016, **334**, 23–33.
- 38 R. Long, H. Huang, Y. P. Li, L. Song and Y. J. Xiong, *Adv. Mater.*, 2015, **27**, 7025–7042.
- 39 R. J. Madix, *Science*, 1986, **233**, 1159–1166.
- 40 M. V. Ganduglia-Pirovano, C. Popa, J. Sauer, H. Abbott, A. Uhl, M. Baron, D. Stacchiola, O. Bondarchuk, S. Shaikhutdinov and H. J. Freund, *J. Am. Chem. Soc.*, 2010, **132**, 2345–2349.
- 41 (a) J. Horiuti and M. Polanyi, *Nature*, 1933, **132**, 819; (b) J. Horiuti and M. Polanyi, *Nature*, 1934, **134**, 377–378.
- 42 Y. Wang, J. Yao, H. R. Li, D. S. Su and M. Antonietti, *J. Am. Chem. Soc.*, 2011, **133**, 2362–2365.
- 43 P. X. Liu, Y. Zhao, R. X. Qin, S. G. Mo, G. G. Chen, L. Gu, D. M. Chevrier, P. Zhang, Q. Guo, D. D. Zang, B. H. Wu, G. Fu and N. F. Zheng, *Science*, 2016, **352**, 797–801.
- 44 G. G. Chen, C. F. Xu, X. Q. Huang, J. Y. Ye, L. Gu, G. Li, Z. H. Tang, B. H. Wu, H. Y. Yang, Z. P. Zhao, Z. Y. Zhou, G. Fu and N. F. Zheng, *Nat. Mater.*, 2016, **15**, 564–571.
- 45 P. Zhai, C. Xu, R. Gao, X. Liu, M. Li, W. Li, X. Fu, C. Jia, J. Xie, M. Zhao, X. Wang, Y.-W. Li, Q. Zhang, X.-D. Wen and D. Ma, *Angew. Chem., Int. Ed.*, 2016, **55**, 9902–9907.